Large irradiation doses can improve the fast neutron/gamma discriminating capability of plastic scintillators

Eva Montbarbon, Marie-Noëlle Amiot, Dominique Tromson, Sylvain Gaillard, Camille Frangville, Romuald Woo, Guillaume H. V. Bertrand, Robert B. Pansu, Jean-Luc Renaud, Matthieu Hamel

Large irradiation doses can improve the fast neutron/gamma discriminating capability of plastic scintillators

Eva Montbarbon,[a,b,c] Marie-Noëlle Amiot,[d] Dominique Tromson,[a] Sylvain Gaillard,[e,*] Camille Frangville,[a] Romuald Woo,[a] Guillaume H. V. Bertrand,[a] Robert B. Pansu,[b] Jean-Luc Renaud[e] and Matthieu Hamel[a,*]

[a] *CEA, LIST, Laboratoire Capteurs et Architectures Electroniques, CEA Saclay, 91191 Gif-sur-Yvette, France.*

[b] *ENS Cachan, 61 avenue du président Wilson, 94230 Cachan, France.*

[c] *Ecole doctorale INTERFACES, Paris-Saclay University, 91300 Saclay, France.*

[d] *CEA, LIST, Laboratoire National Henri Becquerel (LNE-LNHB), CEA Saclay, 91191 Gif-sur-Yvette, France.*

[e] *Normandie University, Laboratoire de Chimie Moléculaire et Thioorganique, 14050 Caen, France.*

Abstract

When new materials appear as potential alternatives for radiation detection, several criteria have to be fulfilled. The one presented herein is the response variation to large irradiation doses of neutron/gamma discriminating plastic scintillators. Thus, several samples were exposed to high gamma doses reaching 10 kGy. They were characterized in terms of gamma spectrometry and fast neutron/gamma discrimination, prior and after irradiation. Results show an unexpected increase of the Figure of Merit (FoM), which is the numerical value for n/γ discrimination performances. An in-depth investigation evaluates the physicochemical impact of such large doses within the material. The characterization includes photophysics, radiation/matter interaction and chemical analyses (EPR, ^{1}H NMR, fluorescence spectroscopy and HRMS).

Introduction

Since 9/11 attacks and the evolution of the war against terrorism, the demand of proportional counter for neutron spectrometry has largely overcome the supply of ^{3}He. These detectors are indeed the gold standard for neutron detection, potentially indicating the presence of nuclear weapons. Since this date, many researchers have turned their attention to ^{3}He detector alternatives. One of these relies on the use of chemically modified plastic scintillators which present the capability of discriminating fast neutrons from gamma rays. In a few words, a plastic scintillator is composed of a polymer matrix, several fluorophores and can be loaded with different molecules, allowing thus numerous formulations. Various strategies have emerged[1] and one promising consists in enhancing the triplet-triplet annihilation inside the material by adding large concentrations (i.e. typically 10 to 20 fold the regular concentration) of the primary fluorophore.

In the path of integrating new materials into improved technologies such as hand-held devices or radiation portal monitors, one has to qualify this material in regards with external or environmental stimuli. Among other material characteristics, plastic scintillator radiation stability is of particular importance, especially when they have been chemically modified with new molecules, and numerous examples have been reported where the material suffered from ageing. Radiation damage studies on plastic scintillators were preliminary studied as early as 1965.[2] The variation of the light yield was studied in regards with gamma dose up to 40 kGy (at 69 Gy/h dose rate) deposited into the scintillator. The consequence of large irradiation doses turns the material to yellow, with a progressive recovery of the initial plastic colorless. Time, temperature and neutral atmosphere are key parameters to recover part or totality of the initial photophysical properties. Zorn showed the beneficial effect of annealing the plastic scintillator with argon to avoid oxidation giving colored centers.[3] Not only the thermal post-treatment appears to be crucial, since heating the material prior to irradiating may lower its radiation hardness, but the causes of this is still unclear.[4] Commercial plastic scintillators EJ-200 (Eljen Technology), BC-404 and BC-408 (Saint-Gobain Crystals and Detectors) were exposed to large irradiation doses from a ^{60}Co source (185 MBq) with a 3162 Gy/h dose rate.[5] Among the three materials, EJ-200 was concluded to have the best behavior. A substantial change of the photophysical response was observed for all samples at a radiation dose of 14.4 kGy. However, it is noteworthy that the previous irradiation step was 602 Gy only, so the behavior of the scintillator may change dramatically between 0.602 and 14.4 kGy.

Different chemical modifications have been reported in literature to enhance material radiation resistance: either by changing the nature of the fluorophore, by loading the material with stabilizers or even by modifying the polymer itself. 3-Hydroxyflavone (3-HF) is a green-emitting, radiation-hard fluorophore. Its favorable Stokes shift is known to virtually prevent any kind of self-absorption within the material.[6] A polyvinyltoluene-based plastic scintillator loaded with *p*-terphenyl and 3-HF was exposed to a 100 kGy total dose (^{60}Co source at 800 Gy/h).[7] When compared with the commercial BC-408 plastic scintillator, the latter was five times more damaged than the PVT/3-HF sample. 3-HF and other flavones were added to polystyrene and exposed to 0.33 kGy (^{60}Co source, 30 Gy/h).[8] The most resistant molecule was 2-([1,1'-biphenyl]-4-yl)-3-hydroxy-4*H*-chromen-4-one.

* Corresponding Authors. E-mail addresses: sylvain.gaillard@ensicaen.fr and matthieu.hamel@cea.fr

A fluorinated 3-hydroxyflavone and its use as a rad-hard dye was also recently reported by the same group.[9]

Poly-2,4-dimethylstyrene[10] exposed to a ^{60}Co gamma source (10080 Gy/h) was shown to recover faster than polystyrene. Authors explain that 2,4-dimethylstyrene macroradicals are highly reactive and more keen to recombine, thus allowing colored centers to vanish.

Also in the objective of introducing new polymers for rad-hard scintillators, the radiation hardness of polyimide-based scintillators loaded with rhodamine B was studied under ion beam induced luminescence and compared to a NE102 commercial sample of same size.[11] Thanks to the higher flexibility of the Si-O bond, polysiloxanes are also potential candidates as rad-hard plastic scintillators.[12]

Another approach is to load plastic scintillators with large amounts of diffusion enhancers, which lead to a better recovery. This strategy was successfully applied to a plastic scintillator loaded with 0.01 % of tin caprylate and 20 % of diphenyloxide, which revealed to retain 91 % of its initial light output after 28 kGy irradiation in air (^{60}Co source, 510 Gy/h).[13] A plastic scintillator is available from Amcrys-H under reference UPS98RH which seems based on this chemical formulation. As a comparison, the UPS923A plastic scintillator, based on a regular composition with 2% *p*-terphenyl and 0.05% POPOP in polystyrene, displays 47% of its initial light yield after 33 kGy.[8] Other diffusion enhancers added to cross-linkers such as 4,4'-divinylbiphenyl (which can act as the primary fluorophore as well) in polystyrene were tested.[14] The best light yield was obtained for *p*-xylene as the diffusion enhancer.

Plastic scintillators exposed to large irradiation doses are usually studied through their absorption and fluorescence characteristics, as well as their scintillation performances. Whereas these macroscopic effects have been extensively studied, to the best of our knowledge the behavior of the material has been poorly described at the molecular state level. Most of the previous work refer to Electron Paramagnetic Resonance[15] (EPR) or mass spectrometry (MS) analyses.[16] Herein, we studied the behavior of plastic scintillators aiming at discriminating fast neutrons from gamma rays. Several lab-made plastic scintillators containing a polystyrene-based matrix and two fluorophores were analyzed before and after high dose irradiation. Irradiation was performed using a Gamma-Cell 220 Excel embedding twelve ^{60}Co sources resulting in a uniform delivered dose at isocenter with 3240 Gy/h air kerma rate. Two scintillators were simultaneously irradiated to reach a cumulative absorbed dose corresponding to an air kerma equal to 10 kGy. In addition to traditional absorption and emission spectra, the irradiated samples were characterized in terms of photoluminescence, time-correlated single photon counting (TCSPC), Time-resolved emission spectroscopy (TRES), gamma-ray pulse height spectra, fast neutron/gamma discrimination, Electron Paramagnetic Resonance response (EPR), thin layer chromatography, and high resolution mass spectra (HRMS). We show that an unexpected behavior occurred as the samples displayed a better Figure of Merit (FoM) while performing the n/γ discrimination after high irradiation dose and different recovery times. An in-depth investigation allows us to formulate different hypothesis about this result. Among them the creation of new chemical species due to radical recombination was explored and evaluated.

Experimental

All the chemicals were purchased from Sigma-Aldrich and used as received unless otherwise stated. Monomers were vacuum-distilled over calcium hydride prior to the experiment. EJ-200 plastic scintillator was obtained from Eljen Technology. The preparation of n/γ discriminating plastic scintillators (ø 25 mm, height 10 mm) is patented.[17] The formulation involved herein can be prepared and resumed according to the following: in a round-bottom flask previously dried and filled with argon, biphenyl, POPOP, 1,4-butanediol dimethacrylate and styrene were mixed altogether. To get rid of residual gases, multiple freeze-pump-thaw cycles were performed. The mixture was allowed to reach room temperature and then poured in a suitable mold, which was sealed under neutral atmosphere and heated. After complete polymerization, the mold was shattered and the free piece was cut and polished until obtaining an optical-grade surface. Ultimately, the scintillator was covered with Teflon® tape to perform gamma spectra and n/γ discrimination experiments.

Fluorescence spectra were recorded in reflection mode with a Horiba Jobin Yvon Fluoromax-4P device, monitored with FluorEssence software. The light decay characteristics of the plastic scintillators were investigated with the TCSPC module available on the Fluoromax-4P spectrofluorometer, with an excitation laser diode operating at 274 nm. Decay spectra were fitted using DAS6 software (Horiba Jobin Yvon). Radioluminescence spectra were acquired by using the following procedure. In the Fluoromax 4P spectrofluorometer, the excitation light was shut down. In the center of the experimenter chamber, a ^{90}Sr/^{90}Y β emitting source (37 MBq) was placed in close contact with the scintillator which opposite side faces the detection cell. Spectra were acquired with integration time 0.1 s/nm.

Absorption/transmission spectra were recorded at room temperature with a Jenway 6715 UV/Vis spectrometer.

^{1}H NMR spectra were recorded on 400 MHz and 500 MHz Bruker spectrometers.

In order to measure their fast neutron/gamma discrimination ability, scintillators were coupled using RTV141A optical grease to a Hamamatsu R7724-100 photomultiplier tube fed with a CAEN N1470 high voltage operating in negative mode. For better comparison the high voltage was kept constant. The {scintillator + PMT} system was placed in front of a ^{252}Cf source (1.85 MBq activity). The anode signal fed a CAEN DT5743 digitizer. Scintillation pulses were then recorded and post-processed. A charge-comparison method has been implemented and the mean Figure of Merit (i.e. for all incident energies) was calculated. Offline treatment allowed the estimation of fast and slow decay times of neutron pulses, as well as their relative intensities.

Gamma-ray spectra were recorded as follows: the sample was optically coupled to a Hamamatsu R7724-100 photomultiplier. A 387 kBq ^{137}Cs radioactive source was used to excite the material. Pulses coming from the PMT were sorted and treated with a custom-made electronic board. The high voltage was kept constant during the experiments as well. Determination of the Compton edge (CE) position was evaluated at 50 % of the decrease of the signal.

Irradiation experiments were performed using a GammaCell® 220 Excel (MDS Nordion Canada) irradiator installed at LNHB (Laboratoire National Henri Becquerel). The GammaCell® air kerma rate was calibrated using an EPR alanine dosimetry method and the LNHB ^{60}Co reference beam[18] according to the IAEA TRS-398 reference protocol.[19] This equipment uses 12 ^{60}Co sources encapsulated in aluminum and stainless steel tubes, fixed within a lead shield. The GammaCell exposure chamber has a cylindrical geometry with 20 cm height and 7 cm radius. The air kerma rate at isocenter at the date of experiments was 3240(20) Gy/h.

The GammaCell® isodose has been experimentally determined and confirmed using the Monte Carlo simulation code MCNP.[20] A cut of the isodose mapping is presented in Figure 1. The plastic scintillators are maintained in a PMMA housing during the experiment in order to assure an electronic equilibrium.

Spectra of radicals created within the plastic scintillator by ^{60}Co irradiation were measured using Electronic Paramagnetic Resonance (EPR). This technique was discovered by Zavoisky[21] and is a well-known technique for free-radical research.[22] It is used in the present work to study the decay of radicals and EPR spectra behavior of the irradiated plastic scintillators against time in regards to the discrimination recovery study. In the literature, EPR has already been reported on EJ-200 (regular) and EJ-260 (green-emitting) plastic scintillators.[15c] Herein, the irradiated scintillator samples were measured using a Bruker Elexsys E500 spectrometer equipped with an ER 4119 HS resonator which was operated in the X-band. The scintillator sample was introduced in a Suprasil quartz tube installed in a holder equipped with a goniometer which allows rotation at different angles of the sample in the cavity (0, 120 and 240°) and makes it possible to average out any "orientation" effects which may be caused by a heterogeneous sample. EPR measurements were performed at a regulated room temperature of 20 ± 2 °C and humidity of 40 ± 10 % RH. The spectrometer settings were selected to optimize the recording of the EPR spectra, which were acquired at the center field of 350 mT with a sweep width of 28 mT. The microwave frequency was ≈ 9.8 GHz. The modulation amplitude and frequency were 0.3 mT and 100 kHz, respectively. The microwave power was 2 mW. 1024 channels per sweep (3 sweeps per measurement) were sampled with a conversion time of 21 ms, the time constant was 82 ms. Each probe was weighed with a microscale (Mettler-Toledo MX5) before EPR measurements. The relative standard uncertainty of plastic scintillator sample weight measurements was 0.01 %. All the spectra of a measurement session were recorded with the same receiver gain. The first derivative of the absorption curve is recorded in order to increase the sensitivity and spectral resolution. The peak-to-peak method was used in order to determine the EPR amplitude of the plastic scintillator sample. The final EPR amplitude is the mean value of the signals of the three angles divided by the sample mass and its associated combined uncertainty. All uncertainties were determined using a coverage factor equal to one.
High resolution mass spectra were obtained with a Xevo G2-XS QTof Waters spectrometer, operating in positive ionization mode.

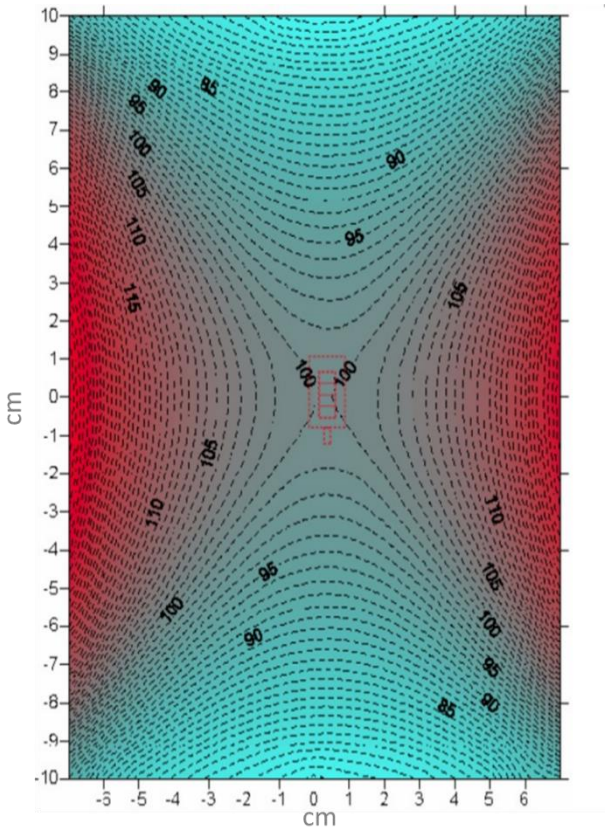

Figure 1. GammaCell isodose mapping.

Results and discussion

Strategy of the experience

The strategy consists in evaluating the influence of large irradiation doses on the photophysical characteristics of both gamma and neutron/gamma discrimination capability of each material. For reference purpose, an EJ-200 commercial plastic scintillator with same dimensions of the modified materials (ø 25 mm, height 10 mm) was irradiated as well. The neutron/gamma discrimination capability was checked by calculating the Figure of Merit (FoM) value prior to irradiation. The scintillators' FoM were measured after each irradiation. Finally, the FoM behavior and the light response of the scintillators were followed for several days after last irradiation. Unfortunately, comparison with a commercial scintillator for neutron/gamma discrimination was not performed, due to the short amount of time available on the GammaCell®.

Preparation of the plastic scintillators

To afford a better understanding of the chemical processes occurring during the irradiation step, six samples were prepared at the same time, from the same chemicals batch (Table 1). After thorough freeze-pump thaw cycles, the solutions were heated until completion of the polymerization. Two different operators of the team were involved in this preparation. Depending on the operator, a discrepancy between the scintillators' FoM and gamma light yield has been observed. Indeed, when exposed to a ^{252}Cf, neutron/gamma emitting source, one of the six samples displayed an undetectable FoM value and a weak gamma light yield compared with the others (Sample 4 in Table 1). All the materials displayed a maximum of emission wavelength in the range 423 – 426 nm which

is due to the POPOP emission wavelength, and no residual emission of biphenyl at lower wavelengths.

Irradiation of the materials

Despite the fact that the GammaCell® can host up to three samples, the first run was performed with sample 1 only in order to evaluate the behavior of the scintillator under irradiation. Details of this experiment are given in the Table 2.

Table 1. Main characteristics of the samples prior to irradiation tests.

Sample	<FoM> ± 14%	Gamma light yield*
1	0.10	0.347
2	0.10	0.362
3	0.19	0.384
4	0	0.272
5	0.10	0.302
6	0.10	0.368
EJ-200	0	1

* set to unity for EJ-200 sample.

Table 2. Details of the irradiation plan performed on sample 1.

Reference dose	Cumulated absorbed dose (Gy)	Absolute uncertainty at k = 2 (Gy)	Observation
D0	0	0	γ spectrum and n/γ discrimination
D1	99	6	γ spectrum
D2	199	8	γ spectrum
D3	299	8	γ spectrum
D4	402	13	γ spectrum
D5	502	13	γ spectrum
D6	750	14	γ spectrum
D7	998	14	γ spectrum and n/γ discrimination
D8	2248	131	γ spectrum
D9	4982	131	γ spectrum
D10	5982	132	γ spectrum
D11	6981	133	γ spectrum
D12	7981	135	2 γ spectra, including one 2 days after irradiation

Table 3. Details of the irradiation and recovery plan performed on sample 1.

Reference dose	Cumulated absorbed dose (Gy) and recovery time (days)	Observation
D12-2d	7981 Gy + 2 days	γ spectrum
D13	9981 Gy	n/ γ discrimination
D13-5d	9981 Gy + 5 days	n/ γ discrimination

The main expected consequence of such irradiation of the scintillators is the impact on the scintillation yield. For instance, the best radiation-stable scintillator is reported by Senchishin et al.[13] It displays a 9 % scintillation yield decrease only after a 28 kGy dose. The gamma spectrum was recorded after each exposure of sample 1, with D1 to D12 reference dose (see Table 2). The Compton Edge (CE), relative to the light yield, and full width at half maximum (FWHM) values, relative to the energy resolution are determined from gamma spectra and are given in the Figure 2. Both values are given with a relative error of ± 1 channel, not represented in Figure 2. CE curves show a steadily decrease down to D12 dose delivery that represents a light output reduction. The FWHM values (red spots) agree within their uncertainty for all delivered doses and can be considered as constant. Unlike a constant FoM value, the light yield was degraded, as well as the detector's resolution, decreasing thus from 23 % at dose 0 up to 63 % at dose 7.981(135) kGy (D12 in Table 2). In fact, sample 1 loses 60 % of its light yield when irradiated at around 8 kGy. But a partial recovery of the scintillator is observed: the same pulse height spectrum analysis was performed two days after the D12 irradiation, giving D12-2d CE and FWHM results. A 39 % increase of the light yield was noticed, starting from D12. This will be fully described in a following section.

During the irradiation process, an increase of the FoM value with the dose appeared, starting at 0.10 prior to irradiation and finishing at 0.64, 5 days after the last irradiation D13 (hereafter called D13-5d, see Table 3). To the best of our knowledge, a light yield recovery conjugated with an FoM enhancement after high dose irradiation has never been reported previously in the literature. The n/γ discrimination plots, as well as their corresponding vertical projection used for the calculation of the FoM are given in Figure 3. From D0 (no dose received by plastic scintillator) up to D13 (10 kGy) delivered dose, an increase of the FoM of more than 80 % is observed, which is more than significant in regards to the FoM uncertainty. Indeed, the FoM relative uncertainty was estimated from data post-treatment equal to 14 %.

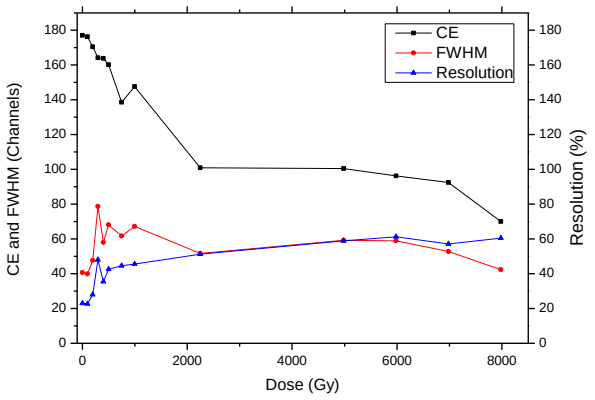

Figure 2. Sample 1 evolution of the Compton edge position (black), the FWHM (red) and the resolution (blue) along with the deposited dose.

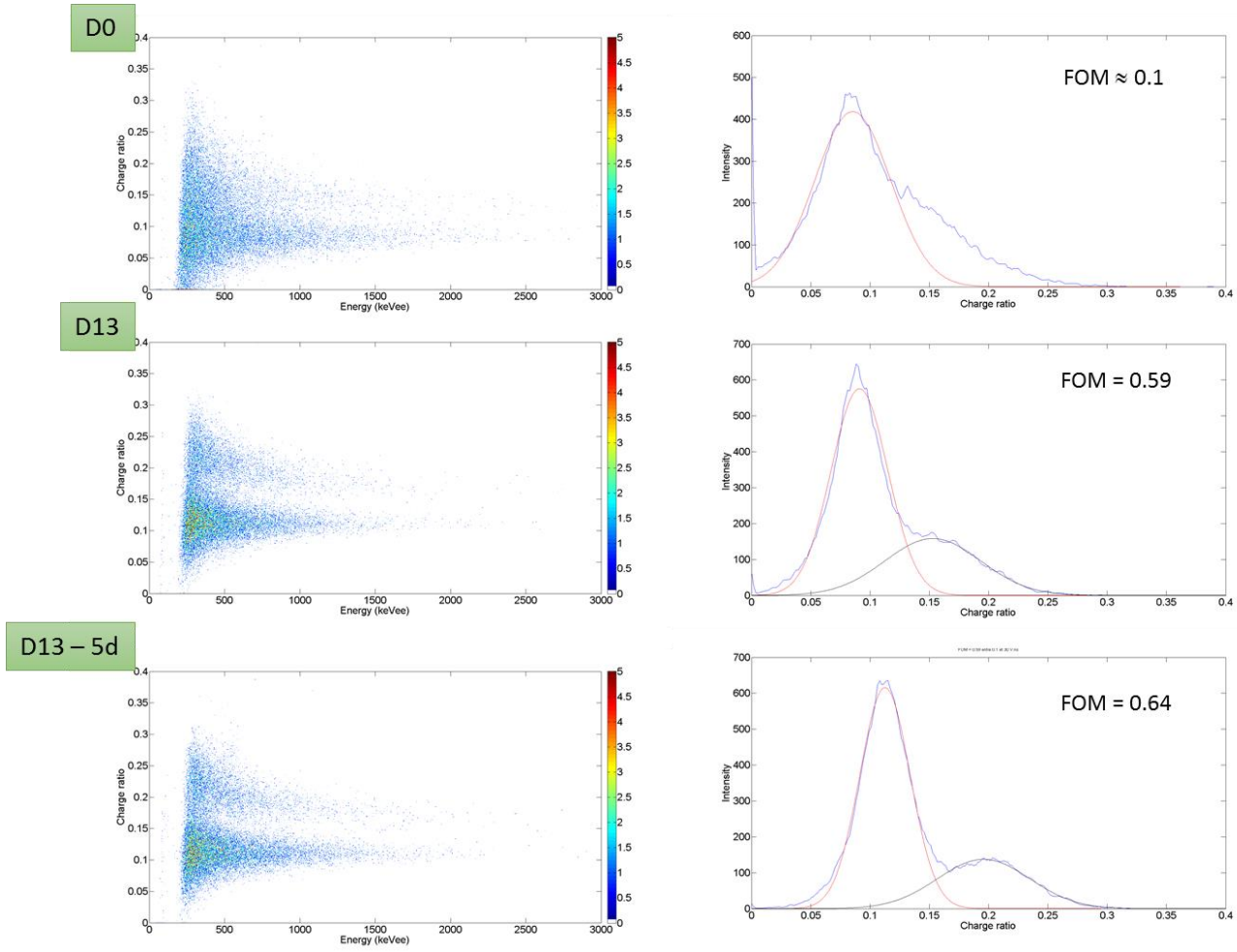

Figure 3. Fast n/γ discrimination plots obtained at various doses and their corresponding summed projection for sample 1.

A second set of experiment considered the irradiation up to 10 kGy of five other samples identically prepared as sample 1 (samples 2 – 6, see Table 1), along with an EJ-200 commercial plastic scintillator. Hence, the samples were characterized at absorbed doses corresponding to air kermas equal to 1.001(13) kGy and 10.00(12) kGy in a cumulative way. After irradiation, the materials were kept under regular conditions, i.e. standard atmosphere, in the dark and at room temperature. The following Figures 4-7 show the evolution of the Compton edge position and the mean value of the Figure of Merit, during and after the irradiation process.

Starting with the mean value of the Figure of Merit, all the samples except sample 4 exhibit a strong increase of the FoM value after irradiation (Figure 4, ± 14 % uncertainty of the FoM, not shown). Despite the fact that sample 4 was prepared along with the others, the FoM value is equal to zero. EJ-200 plastic scintillator was not

added to the Figure 4 as it does not discriminate fast neutrons from gamma rays. All these plastic scintillators were characterized from time to time during almost half a year. During this time, the <FoM> continued to increase until reaching a plateau (Figure 5, ± 1 % uncertainty of the relative light yield, not shown). Even sample 4 started to show a weak FoM. As an example, sample 3 displayed a FoM value of 0.2 before irradiation and 0.75 after irradiation and recovery time.

As the FoM value increased with irradiation process, the relative light yield showed a strong decrease during irradiation. The decrease of the relative light yield was calculated in the range 45 % (EJ-200) up to 70 % (sample 2, Figure 6). During the recovery time, the EJ-200 recovered its light yield almost in its entirety, whereas the chemically modified plastic scintillators recovered around 50 % of their light yield (Figure 7). This fact that EJ-200 plastic scintillator recovered faster than our in-house material is not surprising as it is a weakly loaded scintillator in terms of fluorophores (most likely 1-4 wt%) whereas our materials, loaded over 15 wt% of primary dye.[17] This increases the chance of radical formation on polyaromatic section, which will most likely react to give an optically active byproduct absorbing and lowering the global scintillation yield.

Physical recovery and EPR analysis

As already noticed by several groups, large irradiation doses lead to both visual and detection performance scintillator degradations. However, various parameters can influence the post-treatment of the scintillator and it is known that part of its performances can be recovered. Hypothesis has been made in case of polysiloxane matrix, claiming that flexibility of the Si-O polymer chain increases the chance of bi-radical recombination, hence repairing more efficiently broken bonds. Still, there is no formal explanation about this phenomenon. Figure 8 shows the visual evolution of the plastic scintillators 2 and 3 from 0 up to 10.00(12) kGy and then the recovery performed at room temperature, under air and in the dark up to 7 days after the end of the irradiation. The yellow plastic coloration induced by irradiation progressively disappears with recovery time.

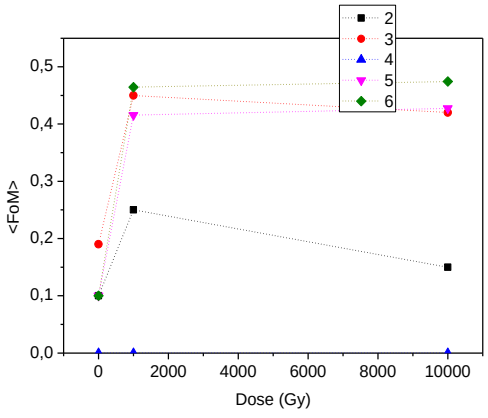

Figure 4. Evolution of the mean value of the FoM at different doses for samples 2 – 6 just after irradiation. The line is drawn to guide the eye.

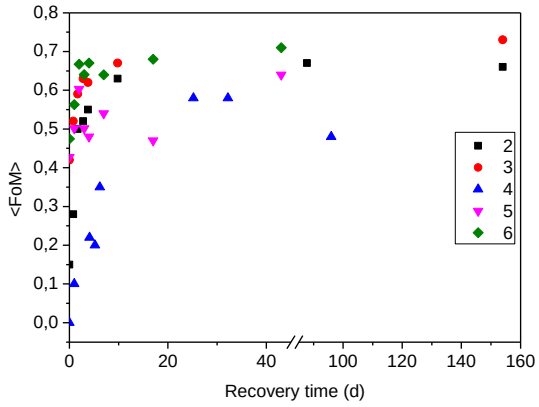

Figure 5. Evolution of the mean value of the FoM after several days of recovery for samples 2 - 6.

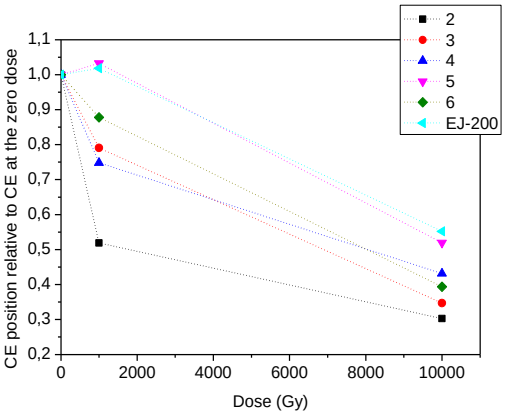

Figure 6. Evolution of the CE position relative to the initial value at different irradiation doses for samples 2 – 6 and EJ-200 plastic scintillator. The lines are drawn to guide the eye.

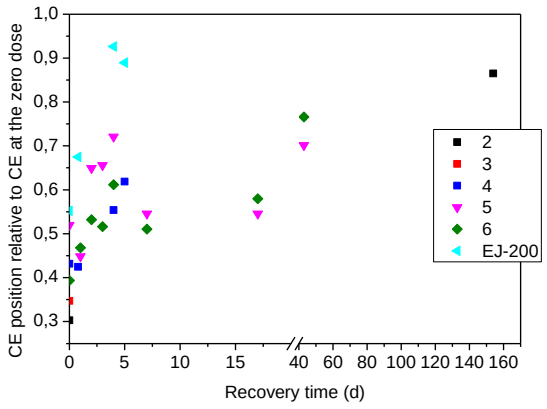

Figure 7. Evolution of the CE position relative to the post-irradiated initial value after several days of recovery, for samples 2 – 6 and EJ-200 plastic scintillator.

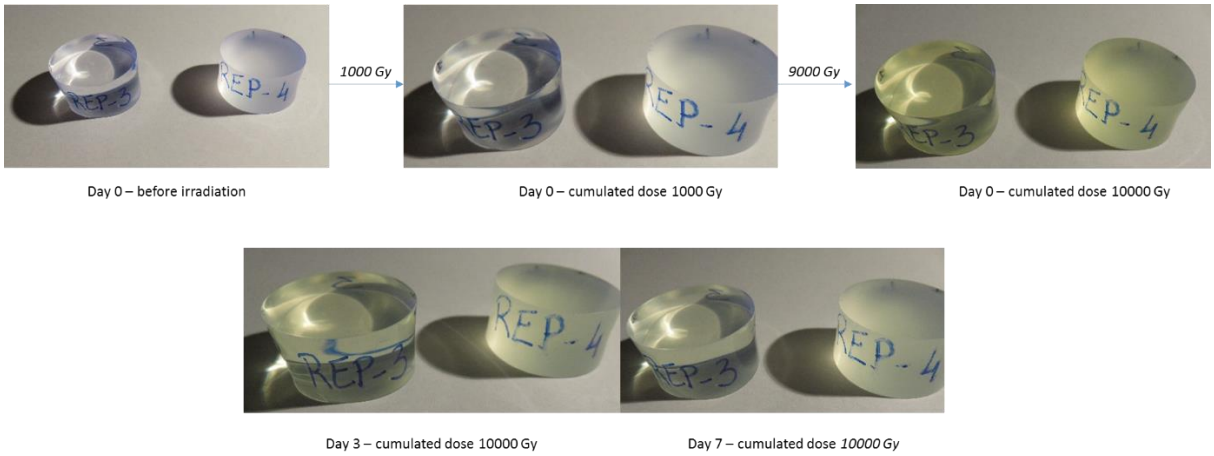

Figure 8. Evolution of the visual aspect of scintillators 2 (left) & 3 (right) from 0 to 10 kGy, then up to 7 days after irradiation. The names REP-3 and REP-4 which are written on the samples represent our internal codification procedure.

Presumably this yellow color is attributed to colored centers, free radicals or even new chemical species. In the context of plastic scintillator irradiation, EPR has been used to detect free radicals creation within the scintillator induced by irradiation and to study their recombination with time.[10] Thus, six small 8 mm^3 cubes were cut from a unique plastic scintillator (hereafter designed as sample 7). Following their irradiation at appropriate dose they were stored at room temperature. 3 pieces of sample 7 (numbered 1 to 3) were irradiated at 1.001(13) kGy, 3 others (numbered 4 to 6) at 10.00(12) kGy and all these samples were then measured by EPR. Figures 9a and 9b present the decay of the amplitude of the EPR signal per sample mass as a function of the post-irradiation time. Uncertainties are very small (below 1 % on the EPR signal for spectra acquired shortly after the irradiation time), that is why they are not drawn on Figure 9b. Concerning the pieces of sample 7 irradiated with a 1.001(13) kGy dose (numbered 1-3), the amplitude of the signal per mass lost 65 % after 7 h and totally disappeared after 29 h (see Figure 9a). By comparison, when the same plastic scintillator was exposed to 10.00(12) kGy, almost 50 % of the radicals were still present after 19 h (Figure 9b). These results can be added to the macroscopic observation that the material takes approximately 5 days to recover (Figure 8), so we can assume that a 10 kGy irradiation leads to creation of a large quantity of radicals, giving colored centers, and their recombination *via* diffusion allows the scintillator to recover from this yellow color. This diffusion is temperature-controlled, as several other groups noticed that the color can be retained when stored at lower temperature than 20 °C.[2,3]

Non irradiated plastic scintillators present no EPR signal whereas irradiated samples present an EPR spectrum which decays with post-irradiation time. Figure 10 shows the EPR spectra of one of the samples irradiated at 10.00(12) kGy as a function of magnetic field. The curves presented in this figure were acquired at different post-irradiation times. EPR spectra are the first derivate of the absorbed signal of the resonance line. The EPR background noise was measured and subtracted to the EPR spectra. Unlike the more straightforward analysis of fluid solution EPR spectra (or single crystals), the interpretation of solid EPR spectra is more demanding, and often complicated by the presence of different paramagnetic active sites, loss of spectral resolution and large line widths. Here the spectra are a result of the contributions of all radicals created by irradiation in their specific orientations with respect to the external field. The peak-to-peak amplitude variation is very low, under 1 %, for measurements acquired at different sample rotation angles (0°, 120° and 240°, respectively) because of the random distribution of the paramagnetic species in the plastic scintillator. Actually, the lack of knowledge of the radical species created by irradiation in the scintillator and of their proportions makes the EPR spectra interpretation very difficult. The stability of the g-factor for all the spectra acquired at different doses and different post-irradiation times may be favorable to the hypothesis that a main radical species is created within the scintillator. Other technics of investigation might be used in order to characterize it.

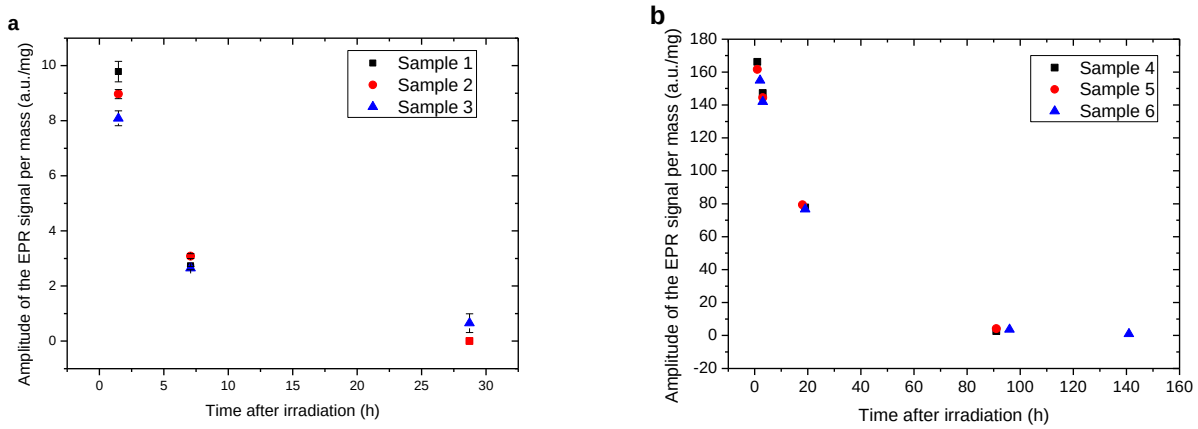

Figure 9. Evolution of the EPR amplitude spectrum per sample's mass with time for two different deposited doses: 1 kGy (a) and 10 kGy (b).

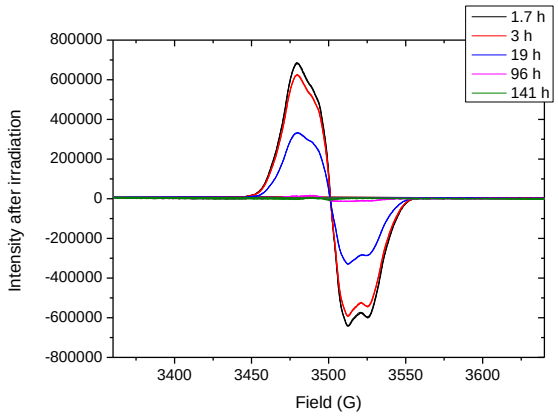

Figure 10. Intensity of the EPR signal as a function of the field for different times after irradiation.

Photophysics

The EPR spectra allowed us to confirm that all free radicals created by irradiation needed a few days to disappear, due to a probable recombination and/or oxidation. To determine which molecules are involved in this process, photophysical experiments were performed on both irradiated and regular samples for a better comparison. Figure 11 shows the steady-state fluorescence spectra comparison of sample 1 prior to and a long time after irradiation, respectively. As one can see, only the response of the secondary fluorophore is visible, which is a traditional trend in organic scintillation, the primary fluorophore's emission being transferred to the secondary dye by Förster energy transfer. However, upon excitation of the material at 280 nm, a bathochromic shift of the response is observed, with the maximum of emission shifting from 424 nm up to 454 nm. These measurements were performed in reflection mode. Spectrophotometry measurements show that before irradiation, the absorption cut-off (wavelength where 10% of light is transmitted) of sample 1 is at 411 nm. A few hours after irradiation, it is shifted at 432 nm with a continuous absorption towards 600 nm. It is noteworthy that the emission spectra of all six materials display the same trend (Figure 12), with emission maxima in the range 448 – 456 ± 1 nm.

This new emission spectrum might be the convolution of POPOP (which is the secondary fluorophore) and an unknown molecule. Given the hypothesis that this new molecule would have a different photoluminescence decay time than POPOP, Time-Resolved Emission Spectroscopy (TRES) was performed on a pristine and on an irradiated sample, in the emission range 410 – 550 nm with the TCSPC module. Two different excitation wavelengths were used: 274 and 368 nm, allowing the probing of the primary fluorophore and the secondary fluorophore responses, respectively. The lifetime of both fluorophores are probed through the POPOP emission, directly in the case of POPOP or after Förster energy transfer for biphenyl. Since the fluorescence of POPOP is shorter than that of its precursor, when excited through biphenyl, POPOP's decay follows that of biphenyl. Biphenyl lifetime increases from 9.8 ± 0.15 ns to 10.4 ± 0.1 ns upon irradiation. POPOP lifetime decreases slightly upon irradiation from 2.25 ns down to 2.05 ns. This was already mentioned to a large extent by Berlman on a red-emissive plastic scintillator exposed to 300 Gy (5 MeV electrons emanating from a LINAC).[23] Colored centers that are created act as quenchers of POPOP. More interestingly, POPOP lifetime depends on the emission wavelength, as it goes longer when shifted to the red. The value $\Delta\tau = \tau_{550\ nm} - \tau_{410\ nm}$ is equal to 0.77 ns for the irradiated sample and 0.47 ns for the safe one. On a side experiment, TRES performed on a diluted POPOP/cyclohexane solution displayed only a moderate decay time shift of 0.01 ns between $\tau_{500\ nm}$ and $\tau_{410\ nm}$. In conjunction with the evolution of the emission spectrum (Figure 12), a hypothesis of the creation of a new molecule may be advanced, but as this molecule has almost the same photoluminescence decay time of POPOP, it could be a POPOP derivative. So, plastic scintillator 1 was sacrificed for further analyses to investigate this hypothesis.

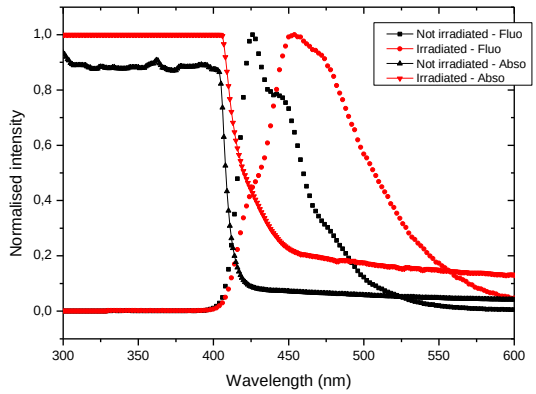

Figure 11. Steady-state absorption (solid lines) and fluorescence (dashed lines) spectra of sample 1 prior to (in black) and after a 10 kGy irradiation (in red). λ_{ex} = 280 nm.

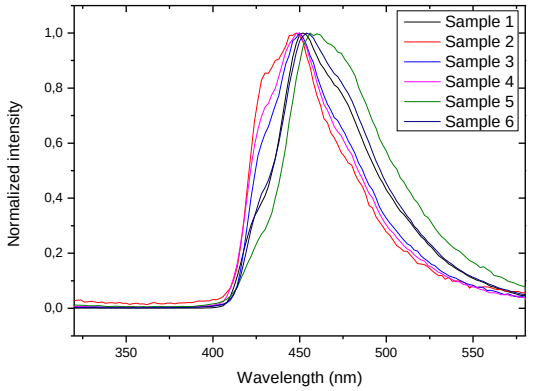

Figure 12. Steady-state fluorescence spectra of samples 1 – 6 (λ_{ex} = 300 nm).

Chemical analyzes

To determine the impact of large doses on the material, an in-depth analysis of an irradiated plastic scintillator was performed. First, sample 1 was grinded in a mortar into a thin powder. The residue was filtered off with methanol and dichloromethane, then the liquid was evaporated to dryness and analyzed.

This filtration was undertaken in order to get rid of the polymer. Literature precedents mentioned that polymer chain scission or cross-linking may occur during and shortly after irradiation.[24] Herein it is assumed that radicals created in the polymer backbone can behave in two different ways. Either they recombine rapidly with other carbon radicals, allowing therefore the polymer to recreate or to cross-link, or upon exposure to diffused oxygen they can be oxidized, giving thus rise to peroxides, which ultimately recombine as well with other radicals. So the second option implies the incorporation of oxygen atoms within the polymer skeleton. This oxidation could explain why the material does not recover 100 % of its initial properties after long-term rest. A better recovery could be reached with a material kept under neutral atmosphere after irradiation.[3] Herein we focus our study only on the effect of large irradiation doses on the fluorophores.

Regarding small molecules, the Thin Layer Chromatography (TLC) analysis with dichloromethane as the eluent gives two different areas, with low and medium polarities. In the low polarity zone (R_f > 0.7), the primary fluorophore was the sole observable product. Even if not observed on the TLC, a biphenyl side-product cannot be excluded. In sharp contrast, the zone with medium polarity (R_f ≈ 0.5) reveals two spots, the largest one comes from POPOP and the second one is an unknown product. LC-HRMS analysis was undertaken on the residual product and Table 4 resumes the main fragments observed. Based on this analysis and data from the literature,[25] a formimide and a formic anhydride derivative are proposed as possible degradation products (molecular peaks at m/z 292 and 293) in the plastic scintillator. A mechanism is presented in Scheme 1 for the formation of both the formimide and the formic anhydride derivative detected in LC-HRMS.[24] As air could be absorbed in the plastic scintillator, the first step might be a formal oxidation reaction, leading to a bicyclic structure containing a peroxide function, via a [4+2] cycloaddition between one oxazole moiety and singlet oxygen under irradiation. POPOP is likely to occur photooxidation, giving this cycloadduct.[26] To account for the color change under irradiation (yellow color of the material disappears slowly after irradiation), we hypothesized that this cycloaddition might be reversible.

Table 4. HRMS main fragments of the formimide and the formic anhydride derivatives.

m/z	Possible fragment
293	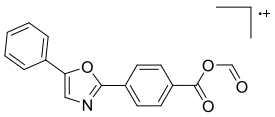
292	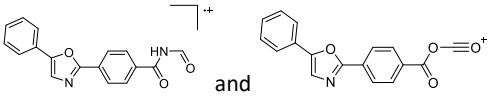
264	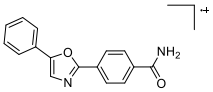
248	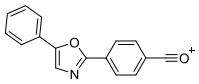
220	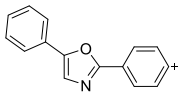
148	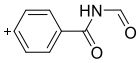

Addition of water on this reactive cycloadduct will deliver the hemiaminal intermediate **I**. As the plastic scintillator is a non-polar, cross-linked polymer, absorption of water seems unlikely. However, this molecule of water might come from the atmospheric humidity during the grinding process of the plastic scintillator. In these conditions, a rearrangement may also lead to intermediate **II**. The two intermediates formed at this stage could then evolve *via* a ring opening reaction (route a and b in Scheme 1, respectively) to the observed formimide (m/z = 292) and formic anhydride derivatives (m/z = 293). These hypotheses are strongly supported by the fragmentation analysis of the HRMS experiment. Indeed, the loss of a CO molecule in the formimide could lead to a radical cation (m/z = 264). Peaks at m/z 292 and 248 might respectively result from a loss

of hydride H• followed by a further loss of CO_2. The hydride loss (m/z = 293 → m/z = 292) might also explain the intensity of the peak at m/z 292. Then, fragmentation of the benzamide radical cation (m/z = 264) and of the phenyl acylium derivative (m/z = 248) might deliver the phenyl cation (m/z = 220). Finally, fragment at m/z 148 might come from the loss of the phenyloxazoline framework from the formimide derivative.

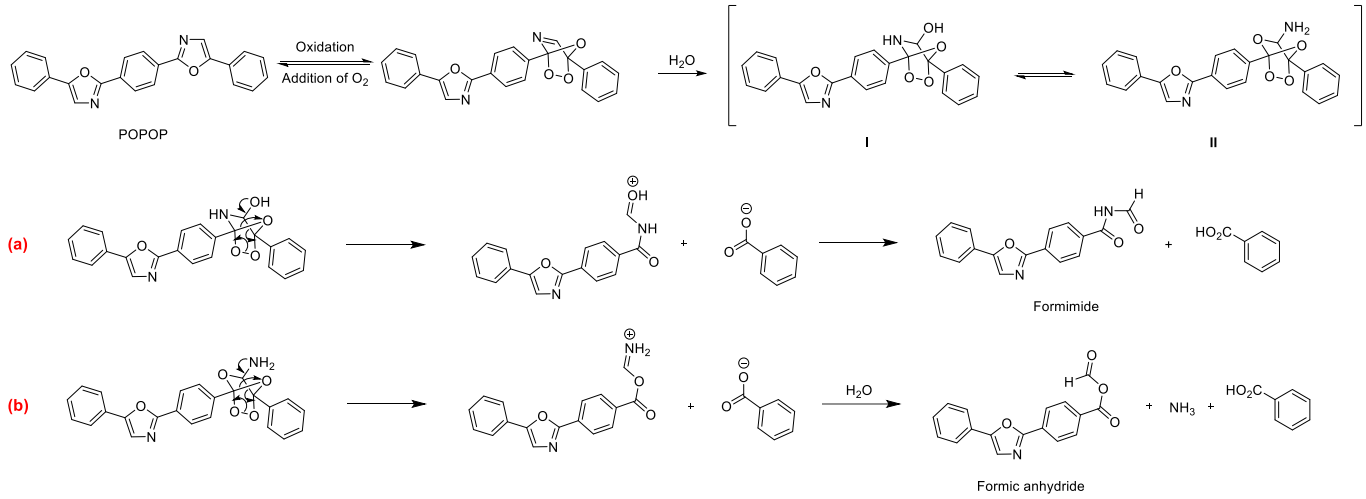

Scheme 1. Proposed mechanism for POPOP degradation under irradiation.

^{1}H NMR analysis was also performed on the small molecules residue. From their polarities, two samples were separated, one with a $CDCl_3$ solution, the other with deuterated methanol. The most polar solution revealed the spectrum of POPOP (major), along with a small proportion of degraded fluorophore. On the other side, the $CDCl_3$ solution is a mix of biphenyl with the presence of an acidic hydrogen which shows a chemical shift near 9.23 ppm, once again at a very low content.

Finally, another irradiated sample was subjected to two successive soxhlet separations, with toluene (first) and isopropanol (second) as the solvent. Thus, the polymer, the toluene- and the *i*PrOH-based solutions were compared to a toluidic solution of POPOP. The results are given in the Figure 13. It is shown that in fact the red-shifted fluorescence fragment is kept trapped inside the polymer backbone – at least in our soxhlet purification process. This could suggest some covalent linking of this fluorescent species to the polymer, so the formimide and/or the formic anhydride are not responsible of this red-shifted fluorescence. So in conclusion, two POPOP derivatives were seen by high resolution mass spectra and ^{1}H NMR, and perhaps another one was linked to the polymer backbone. No relevant information was obtained about the behavior of the biphenyl during the irradiation process.

Conclusions

From this study, we have learnt the capabilities of our materials to handle large irradiation doses such as 10 kGy. Despite the fact that the scintillation yield is largely reduced, an unexpected increase of the neutron/gamma discrimination capability has been observed, for the first time ever.

This irradiation step leads to the creation of several radicals, which are able to recombine as noticed using Electron Resonance Spectroscopy experiments. Several days after irradiation and according to literature precedents, the plastic scintillator is able to recover from this dose. The visual aspect comes from yellow to slight yellow, and the scintillation yield is mostly recovered. Thanks to (photo)chemical analyses, we were able to confirm that such large doses are able to create new chemical species via a probable creation of radicals followed by air oxidation. For the first time new molecular species have been identified post-irradiation, essentially degradation products from the secondary fluorophore. However, this molecule has generally a moderate effect of the FoM value: either by shifting the emitted light if the primary fluorophore in a slightly better way, or the difference between prompt and delayed light might be enhanced. So this cannot fully explain why the scintillators discriminate better, and the soxhlet experiment also showed a shift in the fluorescence of the irradiated polymer, which demonstrates that it has been largely modified as well.

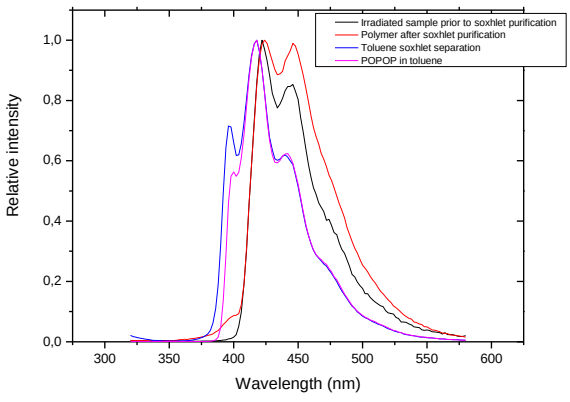

Figure 13. Steady-state fluorescence spectra of an irradiated sample subjected to soxhlet purification, compared with a POPOP solution in toluene (λ_{ex} = 300 nm).

Acknowledgements

We are indebted to the French National Agency "ANR" for financial support, within the frame of the Nessyned project (ANR-15-CE39-0006).

Conflict of interest

The Authors declare no conflict of interest.

References

[1] For a review on this topic, see: Bertrand, G. H. V.; Hamel, M.; Normand, S.; Sguerra, F. *Nucl. Instr. Methods A* **2015**, *776*, 114-128.
[2] Bezuglii, V. D.; Nagornaya, L. L. *J. Nucl. Energy, Parts A/B* **1965,** 19, 490-494.
[3] Zorn, C. *Nucl. Phys. B* **1993,** 32, 377-383.
[4] Johnson, K. F.; Whitaker, H. L. *Nucl. Instr. Methods A* **1991,** 301, 372-375.
[5] Li, Z.; Chong, W.; Yuekun, H.; Xiaojian, Z.; Feng, S.; Zhijia, S.; Jinjie, W.; Zhenghua, A.; Yuda, Z.; Ziping, Z.; Yifang, W. *Nucl. Instr. Methods A* **2005,** 552, 449-455.
[6] Destruel, P.; Taufer, M.; D'ambrosio, C.; Da Via, C.; Fabre, J. P.; Kirkby, J.; Leutz, H. *Nucl. Instr. Methods A* **1989**, *276*, 69-77.
[7] Zorn, C.; Bowen, M.; Majewski, S.; Walker, J.; Wojcik, R.; Hurlbut, C.; Moser, W. *Nucl. Instr. Methods A* **1988,** 271, 701-703.
[8] (a) Gurkalenko, Y. A.; Zhmurin, P. N.; Lebedev, V. N.; Pereymak, V. N.; Svidlo, O. V. *Funct. Mater.* **2016,** 23, (1), 40-44; (b) Velmozhnaya, E. S.; Gurkalenko, Y. A.; Eliseev, D. A.; Zhmurin, P. N.; Lebedev, V. N.; Pereymak, V. N. *Funct. Mater.* **2016,** 23, (4), 650-656.
[9] Gurkalenko, Y. A.; Eliseev, D. A.; Zhmurin, P. N.; Pereymak, V. N.; Svidlo, O. V. *Funct. Mater.* **2017**, *24*, 244-249.
[10] Gunder, O. A.; Voronkina, N. I.; Kopina, I. V. *IEEE Trans. Nucl. Sci.* **1995,** 42, (4), 320-322.
[11] Quaranta, A.; Vomiero, A.; Carturan, S.; Maggioni, G.; Mea, G. D. *Synth. Met.* **2003,** 138, 275-279.
[12] (a) Bowen, M.; Majewski, S.; Pettey, D.; Walker, J.; Wojcik, R. *562 IEEE Trans. Nucl. Sci.* **1989**, *36* (1), 562–566; (b) Quaranta, A.; Carturan, S.; Marchi, T.; Antonaci, A.; Scian, C.; Kravchuk, V. L.; Degerlier, M.; Gramegna, F.; Maggioni, G. *Nucl. Instr. Methods B* **2010**, *268*, 3155-3159; (c) Dettmann, M.; Herrig, V.; Maldonis, J.; Neuhaus, J.; Shrestha, D.; Rajbhandari, P.; Thune, Z.; Been, M.; Martinez-Szewczyk, M.; Khristenko, V.; Onel, Y.; Akguna, U. *J. Instrum.* **2017**, *12*, P03017.
[13] Senchishin, V. G.; Markley, F.; Lebedev, V. N.; Kovtun, V. E.; Koba, V. S.; Kuznichenko, A. V.; Tizkaja, V. D.; Bugadov, J. A.; Belletini, G.; Seminozhenko, V. P.; Zalubovsky, I. I.; Chirikov-Zorin, I. E. *Nucl. Instr. Methods A* **1995,** 364, 253-257.
[14] Velmozhnaya, E. S.; Gurkalenko, Y. A.; Eliseev, D. A.; Zhmurin, P. N.; Lebedev, V. N.; Pereymak, V. N. *Funct. Mater.* **2015,** 22, 494-498.
[15] (a) Alcón, E. P. Q.; Lopes, R. T.; de Almeida, C. E. V. *Appl. Radiat. Isot.* **2005,** 62, 301-306; (b) Pelwan, C.; Jivan, H.; Joubert, D.; Keartland, J.; Liao, S.; Peters, G.; Sideras-Haddad, E. *J. Phys.: Conf. Ser.* **2015**, *645*, 012023; (c) Pelwan, C.; Jivan, H.; Joubert, D.; Keartland, J.; Madhuku, M.; Mellado, B.; Peters, G.; Sekonya, K.; Sideras-Haddad, E. *Proceedings of SAIP2015*, 222-225.
[16] Torrisi, L. *Radiat. Phys. Chem.* **2002,** 63, 89-92.
[17] Hamel, M.; Blanc, P.; Normand, S.; Dehé-Pittance, C. French patent application FR3002945.
[18] (a) Chauvenet, B.; Baltès, D.; Delaunay, F. *Phys. Med. Biol.* **1997,** 42, (11), 2053-2063; (b) Delaunay, F.; Gouriou, J.; Daures, J.; Le Roy, M.; Ostrowsky, A.; Rapp, B.; Sorel, S. *Metrologia* **2014**, 51, 552.
[19] Andreo, P.; Burns, D.T.; Hohlfeld, K.; Huq, M. S.; Kanai, T.; Laitano, F.; Smyth, V. G.; Vynckier, S. IAEA Technical Report Series 398, 2000.
[20] Garcia, T.; Lin, M.; Pasquié, I.; Lourenco V. *Radiat. Phys. Chem*. **2009**, *78*, 782-790.
[21] Zavoisky E. *J. of Phys. (USSR)* **1945,** *3*, (9) 245.
[22] Weil, J. A.; Bolton, J. R. (2006), in Electron Paramagnetic Resonance: Elementary Theory and Practical Applications, Second Edition, John Wiley & Sons, Inc., Hoboken, NJ, USA.
[23] Berlman, I. B.; Ogdan, Y. *Nucl. Instr. and Meth.* **1980,** 178, 411-413.
[24] Celina, M. C. *Polym. Degrad. Stab.* **2013,** 98, 2419-2429.
[25] Rosaria Iesce, M.; Liliana Graziano, M.; Cimminiello, G.; Cermola, F.; Parrilli, M.; Scarpati, R. *J. Chem. Soc., Perkin Trans. 2* **1991**, (7), 1085-1089.
[26] Wasserman, H. H.; Floyd, M. B. *Tetrahedron* **1966**, *22*, (S7), 441-448.